On the monoclinic distortion of β-anhydrite CaSO4

Florian Beaugnon, Sara Quiligotti, Sylviane Chevreux, Gilles Wallez

On the monoclinic distortion of *β*-anhydrite $CaSO_4$

Florian Beaugnon[1,2], Sara Quiligotti[3], Sylviane Chevreux[1], Gilles Wallez[1,2,4]*

[1] Chimie ParisTech, PSL University, CNRS, Institut de Recherche de Chimie Paris, 75005 Paris, France
[2] Centre de Recherche et de Restauration des Musées de France, C2RMF, Palais du Louvre, 75001 Paris, France
[3] Saint-Gobain Research Paris, 39 quai Lucien Lefranc, 93300 Aubervilliers, France
[4] UFR 926, Sorbonne Université, 75005 Paris, France

* corresponding author
gilles.wallez@sorbonne-universite.fr

Abstract: *β*-anhydrite, the stable form of $CaSO_4$, is a common mineral and a key phase in gypsum's dehydration mechanism. An in-depth multi-scale investigation of its structure by powder X-ray diffraction revealed a very slight distortion of the crystal cell at room temperature (β = 90.092(9) °), that led to rule out the commonly admitted orthorhombic model (space group *Cmcm*) in favor of monoclinic *C*2/*c* subgroup. According to high-temperature XRD, the structure resumes however the orthorhombic symmetry around 400 °C.

Keywords: anhydrite; gypsum; crystal structure; phase transition; X-ray diffraction; Rietveld method

Highlights :
- the first evidence of a lattice distortion in β-anhydrite
- a "pseudo tetragonal – pseudo orthorhombic" monoclinic symmetry
- a second-order phase transition is observed around 400 °C

1. Introduction

Anhydrite ($CaSO_4$), that results from the dehydration of gypsum, exists in three forms: the metastable *γ*-anhydrite, the stable and naturally occuring *β*-anhydrite, and *α*-anhydrite which only exists at temperatures higher than 1200 °C. Little is known about the latter, but the structures of both *γ*- and *β*-anhydrite have been described at length in previous works. The crystal structure of *γ*-anhydrite (Fig. 1) is somewhat similar to that of bassanite ($CaSO_4 \bullet ½H_2O$), also obtained by dehydration of gypsum, except that the channels containing the water molecules are empty in the former structure. It crystallizes in the orthorhombic system (space group *C*222) [1] but shows a strong pseudo-hexagonal symmetry around the Ca-SO_4- chains which has led to its description in various space groups. *β*-anhydrite was first identified as "anhydrous sulfated lime" (*chaux sulfatée anhydre*) in 1801 by R.-J. Haüy who wrote "Its mechanical division, similarly perfect in all the directions, results in integrant molecules with a cubic – or nearly – shape" [2], in agreement with its fairly equal cell parameters. The

first radiocrystallographic analysis by Dickson & Binks in 1926 [3] concluded in the orthorhombic symmetry, as would all those that followed.
However, notable progresses have been made in radiocrystallographic instrumentation since the last of these studies, published in the 1980s. The crystal structure is generally described in space group *Amma* [4] or equivalent *Bmmb* [5] (non-standard settings for *Cmcm*, used in the following). It is noteworthy that the [001] Ca-SO_4- chains of the γ-form remain unchanged in the β-form (along [010]), but they re-organize into a dense pseudo-tetragonal array in the latter form (a = 6.99 Å, c = 7.00 Å).

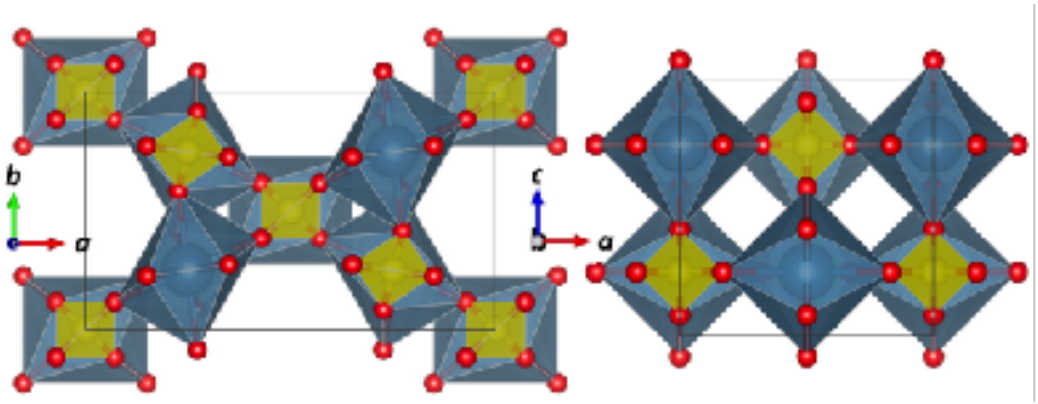

Fig. 1. [001] projection of the crystal structures of γ- (left) and β-anhydrite (right). The corner-connected CaO_8 (blue) and SO_4 (yellow) polyhedra build chains following the projection axis.

As a mineral, *β*-anhydrite is of common occurence in evaporite deposits in association with gypsum and in other environments. Its stability, *i.e.* its low tendency to re-hydration, is due to its lower solubility in water compared to the *γ* form and bassanite. From an industrial point of view, the reactive plaster powder actually consists in a mixture of the two latter phases, obtained by heating gypsum at a temperature of 100-200 °C depending on water vapor partial pressure [6].

Two varieties of hemihydrate, often called “alpha“ and “beta“ plasters (not to be mistaken with the *α* and *β* forms of anhydrite) are commonly distinguished according to their microstructure, in link with their conditions of elaboration. Beta plaster, that results of the calcination of gypsum under dry atmosphere, is made of sub-micron sized crystals with high specific surface, while alpha plaster is prepared by calcination in a wet or hydrothermal environment, resulting in larger crystals with a low specific surface [7,8].

If the material is further heated, *γ*-anhydrite gradually and irreversibly turns into inert *β*-anhydrite, which behaves as a charge during the setting of plaster. It is therefore regarded as undesirable due to its misleading effect on the calculation of the water-plaster mixing ratio and its negative effect on the mechanical properties of the set plaster. Despite its importance, neither the precise mechanism nor the kinetics of the transformation are fully understood, but both the temperature range and the typical time of the transformation are known to be affected by the microstructure [9,10].

In the frame of a multiscale study on the structural mechanisms of the *γ*-*β* transition, the X-ray diffraction (XRD) diagram of the *β* form was carefully examined in order to determine its microstructure. The analysis led however to an unexpected discovery concerning the actual symmetry of this key phase.

2. Experimental

2.1 Samples

Sample 1 to be used for the structural analysis was prepared from a typical “alpha-type“ hemihydrate powder supplied by Saint-Gobain Research Paris (hydrothermal process, grain size 2-20 µm), calcinated at 700 °C for two hours in a muffle furnace, in order to fully transform into *β*-anhydrite [9]. Sample 2, from the same starting material, was heated 3 h at 820 °C, as well as Sample 3, prepared from a ”beta-type” commercial plaster.

2.2 X-ray diffraction

X-ray powder diffraction was conducted on a Panalytical X'Pert Pro diffractometer in Bragg-Brentano geometry with a PIXcel1D detector. The X-ray source was a copper anode vacuum tube and the Cu $K_{\alpha 1}$ emission line was selected with a Ge_{111} monochromator. The instrument was fitted with an Anton Parr furnace for high-temperature measurements. The room-temperature (resp. high-temperature, every 100 °C up to 900 °C) patterns were recorded on a $20 \leq 2\theta \leq 150$ ° ($20 \leq 2\theta \leq 80$ °) range, step 0.013 °, with a total 60 h (70 min) counting time.

2.3 Microstructural analysis

X-ray data for Sample 1 were first processed by Rietveld analysis using the Fullprof suite [11,12] in Le Bail (profile matching) mode, assuming the *Cmcm* symmetry and excluding the overlapping reflections, typically the *hkl* - *lkh* pairs with indexes of the same parity, due to the pseudo-tetragonal symmetry.

In a second step, the whole diagram was refined with cell parameters set at the previously refined values. The peaks FWHM were measured by implementing the Thompson-Cox-Hastings profile function with spherical harmonics expansion to take into account the anisotropy of the microstructure, then checked by single peak or doublet profile fitting. The global broadening β was determined for each peak by substracting the instrumental width measured on a LaB_6 standard, then a Williamson-Hall analysis [13] was performed by plotting $\beta.cos\theta$ against $sin\theta$. Least-squares regression lines were traced for several families including $h00$, $00l$ and $h0l$ in order to calculate the mean crystal dimensions $L_{hkl} = K\lambda/\beta$ from the vertical intercept and the lattice strains ε_{hkl} from the slope.

2.4 Refinement of the crystal structure

The structure of *β*-anhydrite was determined by Rietveld refinement in space group *Cmcm* and in alternative monoclinic symmetry *C*2/*c*. Final reliability factors were (ortho / mono): $\chi^2 = 2.37$ / 2.22, $R_p = 0.072$ / 0.070, $R_{wp} = 0.095$ / 0.092. For the sake of realism, the uncertainties measured by Fullprof were multiplied by 10 for the cell parameters and by Bérar’s factor (2.5) [14] for the intensity-dependent variables.

3. Results and discussion

3.1. Williamson-Hall analysis

The Williamson-Hall plot for Sample 1 on Fig. 2 calls for a careful examination. The $h00$, $00l$ and other reflections with either *h* or *l* null (in the shaded area) exhibit a low strain factor (ε_{hk0}, $\varepsilon_{0kl} < 3.3$

10^{-4}), as expected considering the temperature and duration of the thermal treatment. From the intercept of the *h*00 and 00*l* lines, the crystallites appear to be 200-300 nm wide in the (010) plane, meaning that the large alpha-plaster grains were heavily cracked during firing due to the shrinkage in the (010) plane. This feature is in agreement with the fibrous aspect often observed on natural anhydrite samples of various dimensions.

The other reflections (non-null *h* and *l*) however, are systematically beyond the *h*00 and 00*l* lines. Their slopes are all the higher that, on the one hand, *h* and *l* are close to each other, and on the other hand, *k* is low: the maximal value (13.5 10^{-4}) is reached for the *h*0*h* series.

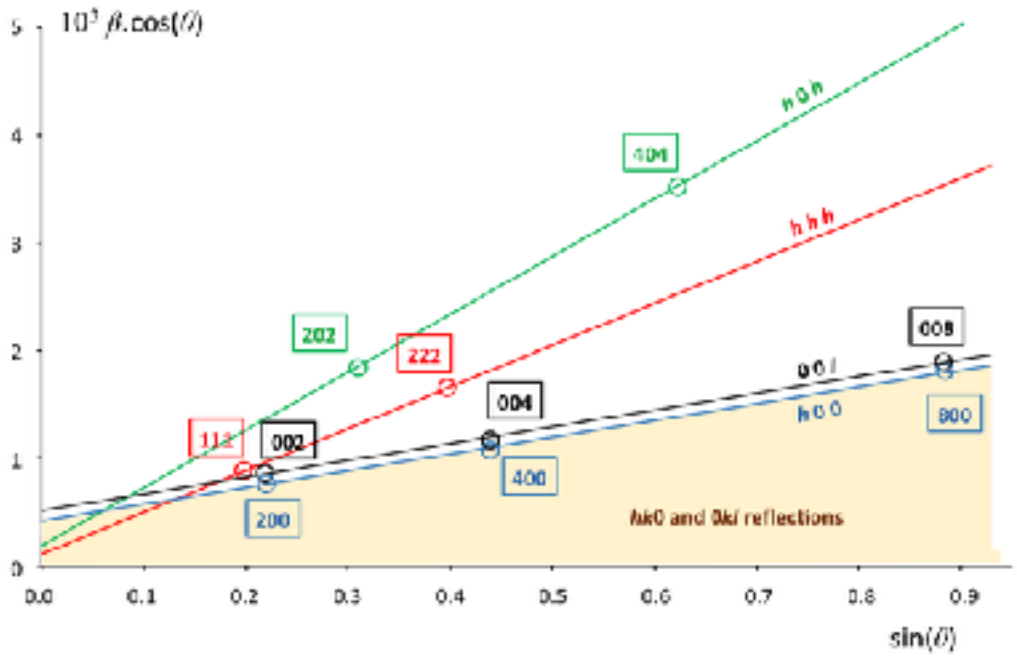

Fig. 2. Williamson-Hall analysis of β-anhydrite (orthorhombic indexing) showing the n^{th} order reflections of the 200, 002, 111 and 202.

For example, a 0.082(5) ° broadening can be measured for the 202 peak in comparison with the narrowest ones of Sample 1. Samples 2 and 3, although prepared at higher temperature (and concerning the latter, from a different material) exhibit a similar (resp. 0.069(5) and 0.071(5) °) widening. The differences between the samples are probably due to microstructural effects.

While clearly inconsistent with a normal strain model, this phenomenon more probably stems from an homogeneous distortion of the crystal lattice. In line with the dependence of the slope against Miller's indexes, a monoclinic distortion in the (010) plane can be considered: the lifting of the degeneracy of the d_{hkl}-d_{-hkl} spacing pairs would actually have no effect should either *h* or *l* be zero, but would yield a maximal splitting if $h = l$ (as $a \approx c$) and if *k* is minimum.

3.2. The monoclinic structure of β-anhydrite

The examination of the extinction rules confirms the *C*-centered lattice and the *c* glide mirror normal to the *b* axis. On this basis, the two possible space groups are *C*2/*c* and *Cc* (n° 9 and 15), subgroups of *Cmcm*. Structure refinements with both groups lead to atomic positions (Table 1) indistinguishable from those in the *Cmcm* symmetry considering the standard uncertainties, therefore *C*2/*c* was retained as the highest possible symmetry (See Fig. 3 for the final Rietveld plot).

The cell parameters remained unchanged, except for β = 90.092(9) °. Note that β can be also infered from the strains measured following *h*0*h* and *h*00 ($\beta \approx \pi/2 + 2\,(\varepsilon_{h0h} - \varepsilon_{h00})$, details in Supplementary Data), giving $\beta \approx 90.12$ °, in fair agreement with the Rietveld measurement. This near-90 value explains why the monoclinic distortion was not discovered until this work.

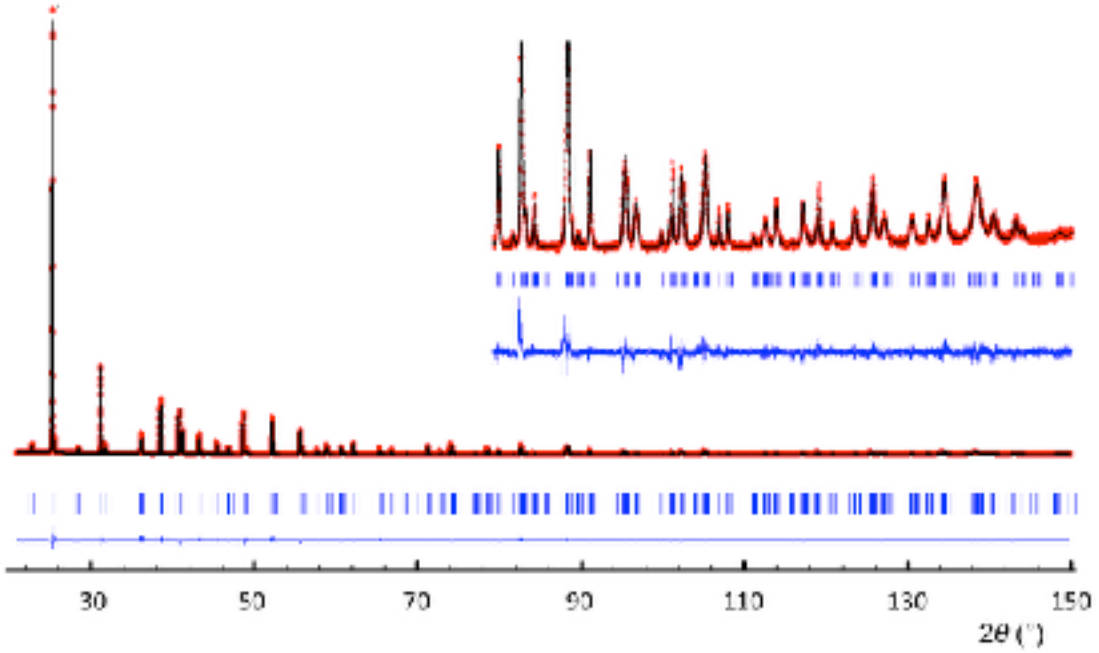

Fig. 3. Rietveld plot for the structure refinement in C2/c symmetry: observed (red dots), calculated (black line), difference (blue line) and Bragg positions (bars). Inset: high-angle x 20 vertical magnification of the 80-150 ° range.

atom	symmetry	*x*	*y*	*z*	B_{eq} (Å²)
Ca	2	0	0.3478(4)	3/4	0.6(1)
S	2	0	0.1560(6)	1/4	0.8(2)
O1	1	0.1695(9)	0.0150(8)	0.252(2)	1.2(3)
O2	1	0.003(3)	0.2979(9)	-0.5805(9)	0.9(3)

Table 1. Atomic positions and displacement parameters refined in space group C2/c, unit cell parameters a = *6.9924(3) Å,* b = *6.2396(3) Å,* c = *7.0001(3) Å and* β = *90.092(9) °.*

3.3. Phase transition

According to the literature, neither differential thermal analysis [15] nor X-ray diffraction [16-18] show any sign of a phase transition until the formation of the face-centered cubic α-anhydrite around 1200 °C. Most of these works are now ancient however, and did not benefit of the improvements in instrumentation that allowed to reveal the monoclinic distortion. The HTXRD data measured in this work can be used to monitor the evolution of the β angle, but the Rietveld analysis of the whole diagrams proved hazardous, as minor imperfections in the sample's surface orientation and the thermal expansion of the holder (despite corrected) do not allow to measure the peaks profile as precisely as with the ambient-temperature mounting. Besides, changes in the microstructure could occur on heating and modify the profile. Although no sintering occured during the experiment, a faint densification of the powder sample was observed afterwards. However, all these biases proved systematic for a given pattern, thus allowing to correct the measured FWHM of a ±*hkl* doublet by substracting the FWHM of a neighbor non-split peak. Fig. 4, obtained by applying this procedure to the sensitive ±202 doublet (2θ = 36.29 ° at RT), corrected by the 310 singlet (41.31 °), gives a clear evidence of the degeneracy of the doublet around 400 °C – a clue for a probable change to the orthorhombic symmetry. As the extinction rules remain unchanged, the space group of this new modification is probably the *Cmcm* supergroup once ascribed to the ambient form. This typical 2nd order phase transition associated to an extremely faint displacive mechanism was not observed by DTA conducted in the frame of this work.

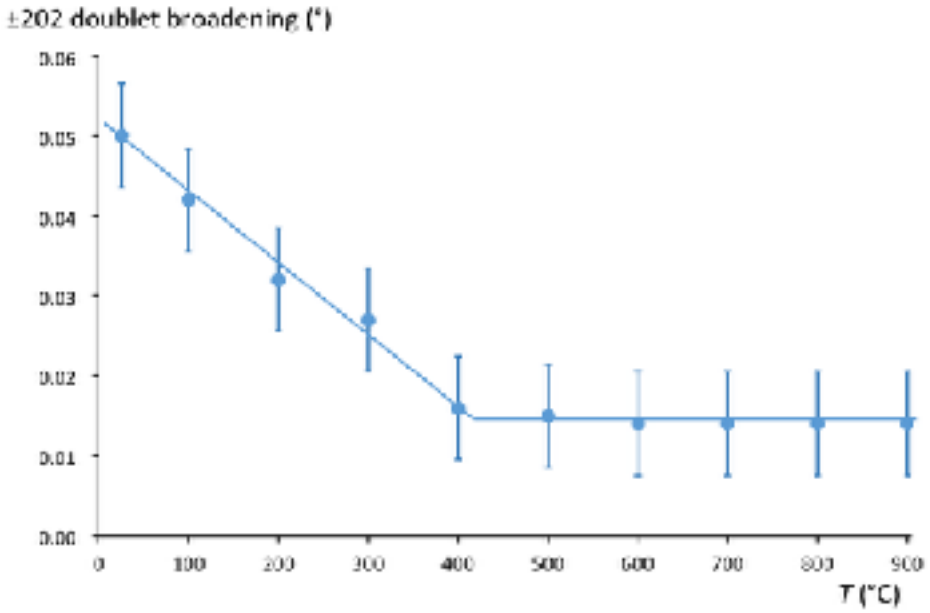

Fig. 4. Thermal evolution of the broadening of the ±202 doublet ($FWHM_{\pm 202} - FWHM_{310}$) evidencing the change in symmetry.

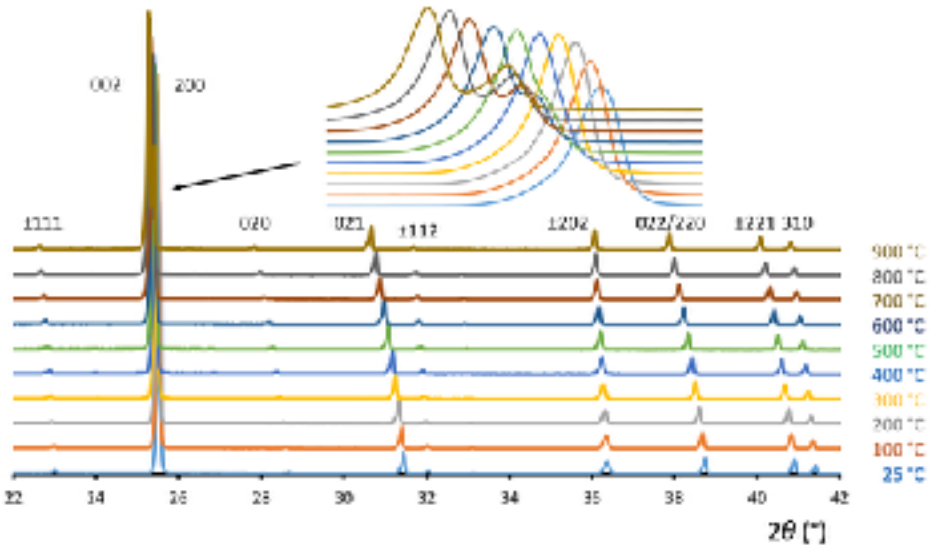

Fig. 5. High-temperature XRD patterns of β-$CaSO_4$, with zoom on the 002/200 doublet.

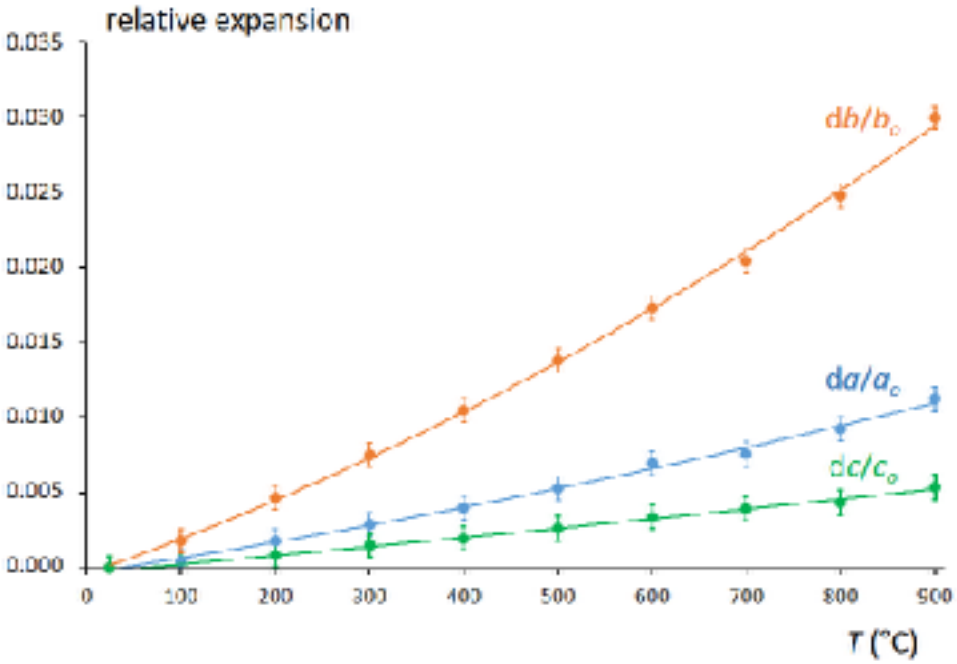

Fig. 6. Thermal expansion plots measured by HTXRD.

Besides the modification of the peaks profile, the transition is too tenuous to be visible on the high-temperature XRD patterns (Fig. 5) or on the thermal expansion plots (Fig. 6) derived by Rietveld analysis. These plots are similar to those reported by Ballirano and Melis [18], who also noted that the strong expansion along [010] resulted from the stretching of the CaO_8 polyhedron. To complete their statement, we can suggest that this phenomenon is due to Coulombic repulsions between Ca^{II} and S^{VI}, which share oxygen edges along the [010] chains.

Unlike the long-hidden pseudo-orthorhombic character of the ambient-temperature form, its pseudo-tetragonal aspect can be easily observed through the quasi-degeneracy of the *hkl*/*lkh* pairs. Actually, the [010] Ca-SO_4- chains form a quasi-square-based array and both the SO_4 and CaO_8 polyhedra almost comply with a -4*m*2 point symmetry, but polyhedra of adjacent (010) layers are equivalent through the *c*-glide mirror in the (100) planes and through the *C*-translation in the (001) planes, thus ruling out any four-fold symmetry. Like those of the literature [17,18], the present HTXRD measurements actually show an increase of the *hkl*/*lkh* splitting on heating due to differences in the mechanism of thermal expansion (Fig. 5). For these reasons, the existence of a tetragonal variety between the orthorhombic β and the cubic α ones is very improbable.

4. Conclusion

During the past decades, advances in XRD instrumentation have allowed to re-explore the symmetry of numerous inorganic compounds, such as γ-anhydrite, and now β-anhydrite. The present work was based upon an unconventional - and unexpected - implementation of the Williamson-Hall analysis, which appeared as a convenient and easy way to detect and even measure a lifting of degeneracy. Of course, synchrotron powder diffraction could be implemented in future works to observe this distortion in a more accurate and straightforward way. To this date, most of the crystallographic studies on β-anhydrite were performed on single crystals obtained from natural samples, which can grow bigger than the sub-micron wide needles resulting from the calcination of plaster, like in the present case. Considering the progress achieved in the past decades in four-circle diffraction, re-visiting this approach with modern instruments could also be an excellent way to improve our knowledge of this phase.

The monoclinic, probably *C*2/*c* ambient structure of β-anhydrite is extremely similar to the previously assumed orthorhombic structure; it is therefore expected that most properties of anhydrite are not significantly affected. However, as slight as it is, this distortion is of importance for studies on the microstructures of β-anhydrite insofar as the lifting of degeneracy of the $\pm hkl$ pairs now allows to conduct fine characterizations based on diffraction peaks profiles. In addition, twin laws depend on the crystal symmetries and pseudo-symmetries. Indeed the main twinning direction of anhydrite is {101} [19], reflecting the tetragonal pseudo-symmetry, but the lifting of the orthorhombic symmetry on cooling should also lead to {100} twins, investigated in a further study.

Declaration of competing interest

The authors declare that they have no known competing financial interests or personal relationships that could have appeared to influence the work reported in this paper.

Acknowledgments

Financial support was received from the LabEx MATISSE and Saint-Gobain Research Paris. The authors also thank Saint-Gobain Research Paris for providing the alpha plaster sample, Doctor

Pascal Loiseau of IRCP-Chimie ParisTech for his precious help in HTXRD experiments and the three anonymous reviewers whose relevant remarks helped improving the article.

Appendix A: Supplementary data

Detailed versions of the Williamson-Hall plots, an alternative calculation of the β angle, thermal expansion equations, interatomic distances and angles and the CIF file are available in the Supplementary data section.

References

[1] C. Bezou, J.-C. Mutin, A. Nonat, Investigation of the crystal structure of γ-$CaSO_4$, $CaSO_4 \cdot 0.5H_2O$ and $CaSO_4 \cdot 0.6H_2O$ by Powder Diffraction Methods, J. Solid State Chem. 117 (1995) 165-176. 10.1006/jssc.1995.1260

[2] R.J. Haüy, Traité de Minéralogie, vol. 4, Conseil des Mines ed., Paris (1801) 348-353. https://gallica.bnf.fr/ark:/12148/bpt6k3898g.texteImage

[3] E.C.S. Dickson, W. Binks, The crystalline structure of anhydrite, Phil. Mag. 2 (1926) 114-128. 10.1080/14786442608564042

[4] S.M. Antao, Crystal-structure analysis of four mineral samples of anhydrite, $CaSO_4$, using synchrotron high-resolution powder X-ray diffraction data, Powder Diff. 26 (2011) 326-330. https://doi.org/10.1154/1.3659285

[5] P. Hartman, On the unit cell dimensions and bond lengths of anhydrite, Eur. J. Mineral. 1 (1989) 721-722. 10.1127/ejm/1/5/0721

[6] J.G.D. Preturlan, L. Vieille, S. Quiligotti, L. Favergeon, Comprehensive thermodynamic study of the calcium sulfate-water vapor system. Part 1: experimental measurements and phase equilibria, Ind. Eng. Chem. Res. 58 (2019) 9596–9606. 10.1021/acs.iecr.9b00857

[7] S. Follner, A. Wolter, A. Preusser, S. Indris, C. Silber, H. Follner, The setting behaviour of α- and β-$CaSO_4 \cdot 0.5H_2O$ as a function of crystal structure and morphology, Cryst. Res. Technol. 37 (2002) 1075-1087. https://doi.org/10.1002/1521-4079(200210)37:10<1075::AID-CRAT1075>3.0.CO;2-X

[8] S. Takahashi, K. Setoyama, SEM observation of β-calcium sulfate hemihydrate particles II. Effects of raw gypsum and condition of production on internal microstructure, Gypsum & Lime 220 (1989) 135-141. https://doi.org/10.11451/mukimate1953.1989.135

[9] S.D.M. Jacques, A.G. Gonzalez-Saborido, O. Leynaud, J.-B. Bensted, M. Tyrer, R.I.W. Greaves, P. Barnes, Structural evolution during the dehydration of gypsum materials, Min. Mag. 73 (2009) 421-432. 10.1180/minmag.2009.073.3.421

[10] C. Mitsuki, M. Kita, Transition of calcium sulfate hemihydrate to insoluble anhydrite, Nature 184 (1959) 1481. 10.1038/1841481a0

[11] J. Rodriguez-Carvajal, Recent developments of the program FULLPROF, Commission for Powder Diffraction (IUCR) Newsletter 26 (2001) 12-19.

[12] J. Rodriguez-Carvajal, T. Roisnel, FullProf 98 and WinPLOTR: New Windows 95/NT Applications for Diffraction, Commission for Powder Diffraction (IUCR) Newsletter 20 (1998) 35.

[13] G.K. Williamson, W.H. Hall, X-ray line broadening from filed aluminum and tungsten Acta. Metall. 1 (1953) 22-31. 10.1016/0001-6160(53)90006-6

[14] J.-F. Bérar, P. Lelann, E.S.D.'s and estimated probable error obtained in Rietveld refinements with local correlations, J. Appl. Crystallogr. 24 (1991) 1-5. 10.1107/S0021889890008391

[15] R.R. West, W.I. Sutton, Thermography of Gypsum, J. Am. Ceram. Soc. 37 (1953) 221-224. 10.1111/j.1151-2916.1954.tb14027.x

[16] O.W. Flörke, Die Hochtemperaturmodifikationen von Kalzium-, Strontium- und Bariumsulfat, Naturwis. 39 (1952) 478-479. 10.1007/BF00592322

[17] H.T. Evans, The thermal expansion of anhydrite to 1000 °C, Phys. Chem. Minerals 4 (1979) 77-82. 10.1007/BF00308361

[18] P. Ballirano, E. Melis, Thermal behaviour of beta-anhydrite $CaSO_4$ to 1263 K, Phys. Chem. Minerals 34 (2007) 699-704. 10.1007/s00269-007-0186-2

[19] J.W. Anthony, R.A. Bideaux, K.W. Bladh, M.C. Nichols, Handbook of Mineralogy, Mineralogical Society of America, Chantilly, VA 20151-1110, USA. http://handbookofmineralogy.org/

Supplementary data

1. X-ray diffraction

1.1. Polynomial fit of the instrumental FWHM function

$FWHM\ (°) = 8.9704\ 10^{-8}\ (2\theta)^3 - 8.4192\ 10^{-6}\ (2\theta)^2 + 3.5065\ 10^{-4}\ (2\theta) + 3.7456\ 10^{-2}$

1.2. h0h peak profile

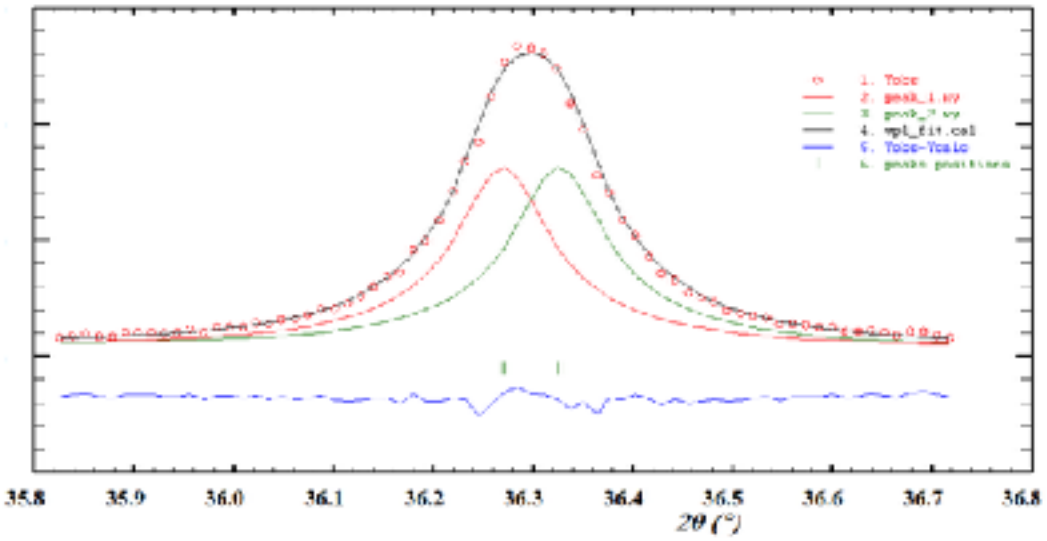

Figure S1. The anomalous profile (Lorentzian-shaped sides and Gaussian-shaped top) indicates a splitting of the 202 reflection.

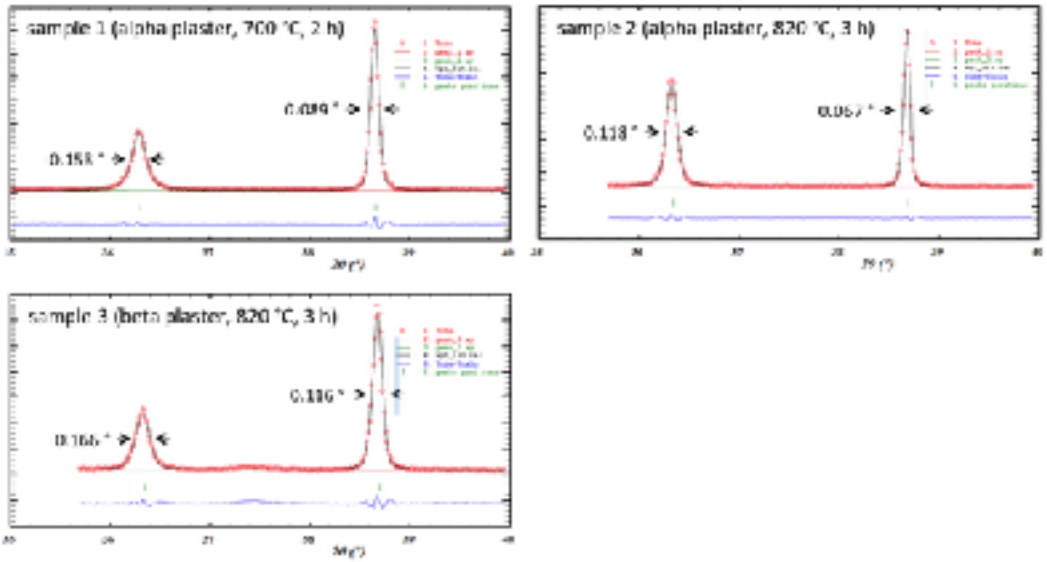

Figure S2. FWHM of the ±202 doublet (2θ = 36.29 °) in Samples 1, 2 & 3. The 022 – 220 doublet (pseudo-tetragonal symmetry) at 2θ = 38.64 °, showned for comparison, is itself broader by about 0.01 ° than the singlet peaks.

2. Williamson-Hall analysis

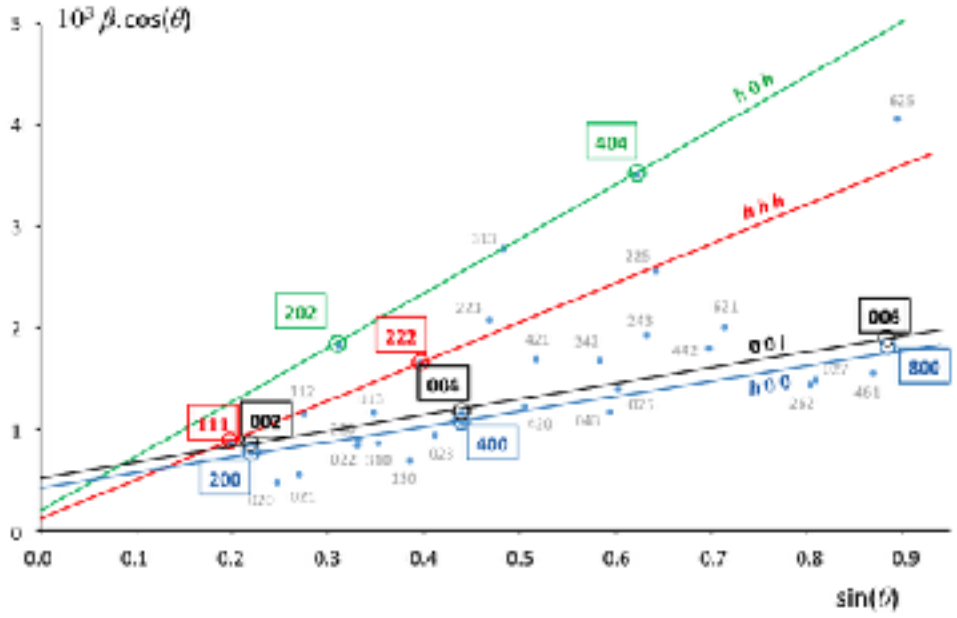

Fig. S3. The complete Williamson-Hall analysis of β-anhydrite based on the orthorhombic indexing.

3. Alternative calculation of the *β* angle

Assuming that the excess in the strain measured for the $h0h$ line (ε_{h0h} - ε_{h00}) results from the lifting of degeneracy between the d_{h0h} and $d_{\text{-}h0h}$ spacings, one can write:

$$\frac{\Delta d}{d} = \frac{\left(d_{h0h} - d_{-h0h}\right)}{2\bar{d}} = \left(\varepsilon_{h0h} - \varepsilon_{h00}\right)$$

In the monoclinic system (unique axis ***b***) and assuming $a \approx c$:

$$d_{h0h} = \frac{a\,.\,sin\beta}{h\sqrt{2}\sqrt{1-cos\beta}} \quad and \quad d_{\bar{h}h0} = \frac{a\,.\,sin\beta}{h\sqrt{2}\sqrt{1+cos\beta}}$$

and $\bar{d} = \dfrac{a}{h\sqrt{2}}$

Considering that $\cos\beta \approx 0$ and assuming limited development

$(1 + \cos\beta)^{-1/2} = 1 - 1/2\ \cos\beta - 3/8\ (\cos\beta)^2 + ...$

one gets

$$\frac{d_{h0h} - d_{\bar{h}0h}}{\bar{d}} \approx sin\beta\,.\,cos\beta$$

Assuming now limited developments for $\beta \approx \pi/2$

$\sin\beta = 1 - (\beta - \pi/2)^2 + ...$ and $\cos\beta = (\beta - \pi/2) + ...$

we get

$$\frac{d_{h0h} - d_{\bar{h}0h}}{\bar{d}} \approx \beta - \pi/2$$

To summarize

$$\beta \approx \frac{\pi}{2} + 2\left(\varepsilon_{h0h} - \varepsilon_{h00}\right)$$

Application $\beta \approx 1.57284$ rad ≈ 90.12 °

4. Structural data

atom	symmetry	*x*	*y*	*z*	*B*eq (Å²)
Ca	*m*2*m* 2	0 0	0.3478(5) 0.3478(4)	3/4 3/4	0.6(1) 0.6(1)
S	*m*2*m* 2	0 0	0.1562(6) 0.1560(6)	1/4 1/4	0.8(2) 0.8(2)
O1	..*m* 1	0.1693(9) 0.1695(9)	0.0148(9) 0.0150(8)	1/4 0.252(2)	1.1(2) 1.2(3)
O2	*m*.. 1	0 0.003(3)	0.2981(9) 0.2979(9)	-0.5805(9) -0.5805(9)	0.8(3) 0.9(3)

Table S1. Comparison between the atomic positions refined in the Cmcm (upper) and C2/c (lower) groups.

bond	length (Å)	multiplicity
Ca-O1	2.555(6) 2.465(6)	2 2
Ca-O2	2.334(6) 2.509(6)	2 2
S-O1	1.476(6)	2
S-O2	1.481(6)	2
bonds	angle (°)	multiplicity
O1-S-O1	106.8(6)	1
O2-S-O2	106.5(6)	1
O1-S-O2	109.9(9) 111.9(9)	2 2

Table S2. Selected bond lengths and angles calculated in the C2/c setting (s. u. multiplied by Bérar's factor = 2.5).

5. Thermal expansion equations

axial relative expansion, with T (°C):

$$\mathrm{d}a/a_{20} = 3.25\ 10^{-9}\ T^2 + 9.63\ 10^{-6}\ T - 3.39\ 10^{-4}$$
$$\mathrm{d}b/b_{20} = 1.24\ 10^{-8}\ T^2 + 2.19\ 10^{-5}\ T - 3.88\ 10^{-4}$$
$$\mathrm{d}c/c_{20} = 7.17\ 10^{-10}\ T^2 + 5.55\ 10^{-6}\ T - 3.18\ 10^{-4}$$